Research Article | Vol. 31, No. 15 / 17 Jul 2023 / Optics Express 23966
Optics EXPRESS

Tunable backward terahertz-wave parametric oscillator centered at a high frequency of 0.87 THz with injection seeding

JOSELITO E. MULDERA,[1,*] KOUJI NAWATA,[1,2] YUMA TAKIDA,[1] DEEPIKA YADAV,[1] AND HIROAKI MINAMIDE[1]

[1]*Tera-Photonics Research Team, RIKEN Center for Advanced Photonics, RIKEN, 519-1399 Aramaki-Aoba, Sendai, Miyagi 980-0845, Japan*
[2]*Department of Information and Communication Engineering, Tohoku Institute of Technology, Sendai, Miyagi 982-8577, Japan*
[*]*joselito.muldera@riken.jp*

Abstract: We report the first demonstration of a frequency tunable backward THz-wave parametric oscillator (BW-TPO) centered at a high frequency of 0.87 THz using a slant-stripe-type magnesium oxide-doped periodically poled lithium niobate (PPLN) crystal as the nonlinear medium. Down-converted THz and idler beams generate upon excitation of the PPLN with a sub-nanosecond pulsed source of λ = 1064.44 nm. The resulting first idler has a wavelength of 1067.75 nm, equivalent to an oscillation frequency of 0.872 THz as per the spectral line separation from the pump. We also present angle tuning of the BW-TPO frequency ranging from 0.836–0.905 THz through PPLN rotation. The threshold pump intensity for BW-TPO is determined to be 5.6 GW/cm^2 while obtaining a conversion efficiency as high as 12.3% at a pump energy (intensity) of 15.25 mJ (8.90 GW/cm^2). A reduction of the BW-TPO threshold energy and improved pump-to-idler energy conversion efficiency resulted from injection seeding with a CW laser at the same wavelength as the first idler. The THz output is also directly proportional to seed power.

© 2023 Optica Publishing Group under the terms of the Optica Open Access Publishing Agreement

1. Introduction

The quest to discover and create sources capable of bridging the so-called THz-gap is one of the primary areas of focus in terahertz research. The potential applications of these THz sources, including the next generation of telecommunications and imaging, are fueling the interest in this field [1–5]. The sub-THz frequency range is particularly relevant for the aforementioned applications due to its high transparency in materials, excellent directivity, and relatively high resolution. Nonlinear optical crystals, when pumped with a laser, represent a well-established group of THz sources, with lithium niobate (LN) being a key photonic material of interest due to its large nonlinear coefficient and ease of engineering [5]. The absorption of THz radiation in LN is known to decrease with decreasing sub-THz frequencies, making it a candidate for the previously mentioned applications. To generate THz-waves using lithium niobate, various configurations have been executed based on different physical mechanisms: tilted pulse front [6], singly resonant optical parametric oscillation (OPO) [7], difference frequency generation (DFG) [8], optical parametric generation (OPG) [9], and of particular interest in this present work, is in its use in backward optical parametric oscillation (BW-OPO). The concept of BW-OPO was initially proposed by Harris [10] in the 1960s; it involves a three-wave counterpropagating parametric interaction, where a pump source directed at a nonlinear optical medium gets down-converted through energy conservation into collinear signal and idler beams. The signal beam propagates in the backward direction while the idler beam propagates in the forward direction. The frequency of the generated signal is tunable and lies in the infrared range. The BW-OPO also comes with

#494232 https://doi.org/10.1364/OE.494232
Journal © 2023 Received 26 Apr 2023; revised 7 Jun 2023; accepted 9 Jun 2023; published 6 Jul 2023

Optics EXPRESS

the advantage of being cavityless, providing some leeway in the tightness of the optical alignment when compared with standard OPO. The model by Harris was then extended to generate a submillimeter to THz-waves using an IR pump source through quasi-phase-matching (QPM) with periodically poled lithium niobate (PPLN) as the nonlinear medium [11,12]. However, executing this experimentally has been challenging. Meanwhile, the first experimental demonstration of BW-OPO was reported by Canalias and Pasiskevicius using a submicrometer periodically poled $KTiOPO_4$ (PPKTP) as the gain medium, achieved through the QPM technique [13]. The generated signal lies in the near-infrared while the idler waves are in the mid-infrared range, where further demonstrations of BW-OPO with PPKTP were made by their group [14–17]. Recently, it was experimentally shown that backward THz-wave parametric oscillation (BW-TPO) can be achieved by quasi-collinear phase-matching (QCPM) in a slant-stripe-type PPLN with the readily available grating period (Λ) of tens of microns [18,19], more than two decades after the model [11,12]. The resulting BW-TPO frequency was observed to be angle tunable with crystal rotation. In addition, the first continuous wavelength (frequency) tunable BW-TPO was also presented in [19], realized by injection seeding with a tunable CW laser around the idler wavelength. Moreover, injection seeding, used for OPG, significantly enhanced the overall performance of slant-stripe-type PPLN BW-TPO. It is also worth noting that with injection seeding in THz-wave parametric generators (is-TPG), gyrotron-class peak output powers (kW) have been achieved [20], so its application to BW-TPO is promising. On the other hand, generating THz-waves with higher frequencies around 1 THz is still challenging because of the increased absorption coefficient of LN. Additionally, the grating pitch of the PPLN should be smaller than previously reported. However, for a smaller grating pitch, there may be a possible overlap with other phase-matching conditions that generate mid-infrared radiation, such as OPG, so gain competition needs to be considered. Therefore, the criteria for generating high-frequency THz-waves are not yet clarified.

In this work, we designed a slant-stripe-type PPLN BW-TPO customized to emit THz-waves at a relatively high frequency of 0.87 THz when pumped with a pulsed IR laser, expanding the operation frequency from 0.3 THz previously reported in [18,19]. In addition, we demonstrate the angular tunability of the BW-TPO frequency by rotating the PPLN crystal, and subsequently measure the conversion of pump energy. Injection seeding by a CW source was also carried out to observe its effect on the BW-TPO performance of the slant-stripe-type PPLN device.

2. Materials and methodology

The BW-TPO configuration is shown in Fig. 1(a) along with the corresponding angular momentum vector diagram for QCPM in Fig. 1(b). A small quasi-collinear angle θ between the pump and THz/idler beams is introduced in the phase-matching brought about by the slant angle of the PPLN. There are instances when due to the efficient energy conversion of the pump, a cascading process ensues where more than one idler wave is created; the corresponding angular momentum phase diagram is illustrated in Fig. 1(c). The angle between the pump beam and the grating vector of the PPLN is designated α. From this QCPM scheme, the dependence of the generated THz wavelength on both Λ and α was determined [18] making it possible to engineer the momentum vectors for a target BW-TPO frequency. The relationship between α and THz frequency is shown in Fig. 1(d) for the grating period of 35 μm where this "tuning" curve became the basis for the current slant-stripe-type PPLN design. The effect of injection seeding was also investigated as in [19].

The slant-stripe-type MgO(5 mol%):PPLN crystal medium was engineered with a periodic poling of $\Lambda = 35.0\,\mu$m and a $\alpha = 43.0°$ based on the tuning curve in Fig. 1 (**d**), from the BW-TPO QCPM established in [18]. The PPLN has dimensions of 40.0 (length) x 14.0 (width with 10 mm poling region plus 2 mm blank on both edges for laser damage prevention) x 1.00 (thickness) mm^3 with antireflection coating for the pump wavelength applied to its optically finished facets. A single-longitudinal-mode microchip Nd:YAG pulsed laser with $\lambda = 1064.44$ nm, FWHM pulse

Optics EXPRESS

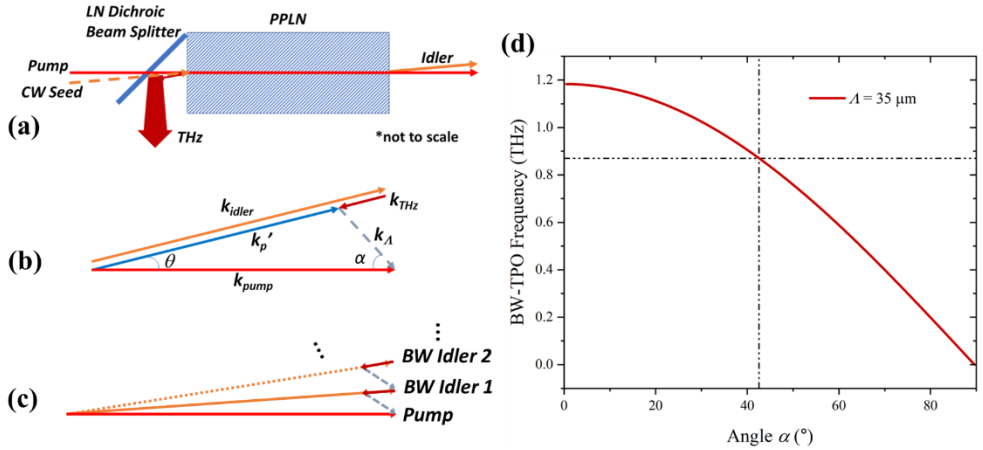

Fig. 1. (a) Schematic of the BW-TPO configuration and experimental setup as viewed from the top. (b) Angular momentum vector phase-matching diagram of BW-TPO with a small quasi-collinear angle θ between the pump and THz/idler beams. (c) QCPM diagram when cascading process is considered. (d) Calculation results for the dependence of the BW-TPO frequency on the angle α at a grating period of $\Lambda = 35$ µm. The dashed crosshairs designate the corresponding α for the target frequency.

width of 0.86 ns, and repetition rate of 20 Hz served to pump the PPLN. The pump beam was collimated by a cylindrical lens pair to an elliptical FWHM beam spot of ~ 850 µm and 295 µm in the horizontal and vertical dimensions, respectively. A tunable CW external-cavity laser diode (SpectraQuest Lab. Inc, λ-master 1040) set at the wavelength of the first backward idler and made to pass through a Ytterbium-doped fiber amplifier (Keopsys, CYFA-PB series) comprise the injection seeder. The seed beam, positioned at an incident angle corresponding to the quasi-collinear angle θ and accounting for refraction, was then made to overlap with the pump beam shown in the schematic of the experimental setup in Fig. 1(a). Both the pump and seed beam polarizations were oriented along the z-axis of the PPLN. The pump and idler beams spatially separate after the PPLN as per the BW-TPO QCPM. The pump energy was varied to observe the BW-TPO threshold and conversion efficiency. A spectrum analyzer with a spectral resolution of 0.01 nm checked for the wavelengths of the pump and idler beams, while an optical energy meter measured the pump and idler energies. The THz signal was separated from the pump and seed beamlines by an originally-developed LN dichroic beam splitter positioned at an angle of incidence of ~45° to be then detected by either a pyro-electric detector or a calibrated Schottky barrier diode. The THz frequency was also confirmed using a scanning etalon consisting of two partially reflecting silicon wafers with one mounted on a translation stage, to vary the distance between the Si mirrors. All experiments were performed at a controlled room temperature of 22°C.

3. Results

3.1. Pump and idler spectra

The spectra of the pump and resulting idler peaks are given in Fig. 2 (a) taken at a pump energy of 15.3 mJ. The forward propagating backward idler resulting from the main BW-TPO phase-matching, noted as BW Idler 1, is at $\lambda = 1067.75$ nm. The spectral separation $\Delta\omega_{BW1}$ from the pump line corresponds to the BW-TPO frequency of 0.872 THz or $\lambda_{THz} = 344$ µm. The measured idler wavelength and BW-TPO frequency are in good agreement with calculations based on the QCPM model in Fig. 1 (b). Indicative of efficient energy conversion, another backward

Optics EXPRESS

idler, BW Idler 2, is observed at $\lambda = 1071.03$ nm due to a cascading process where BW Idler 1 acts as the new pump source and results in a spectral separation $\Delta\omega_{BW2} = 0.862$ THz ($\lambda_{THz} = 347$ µm).

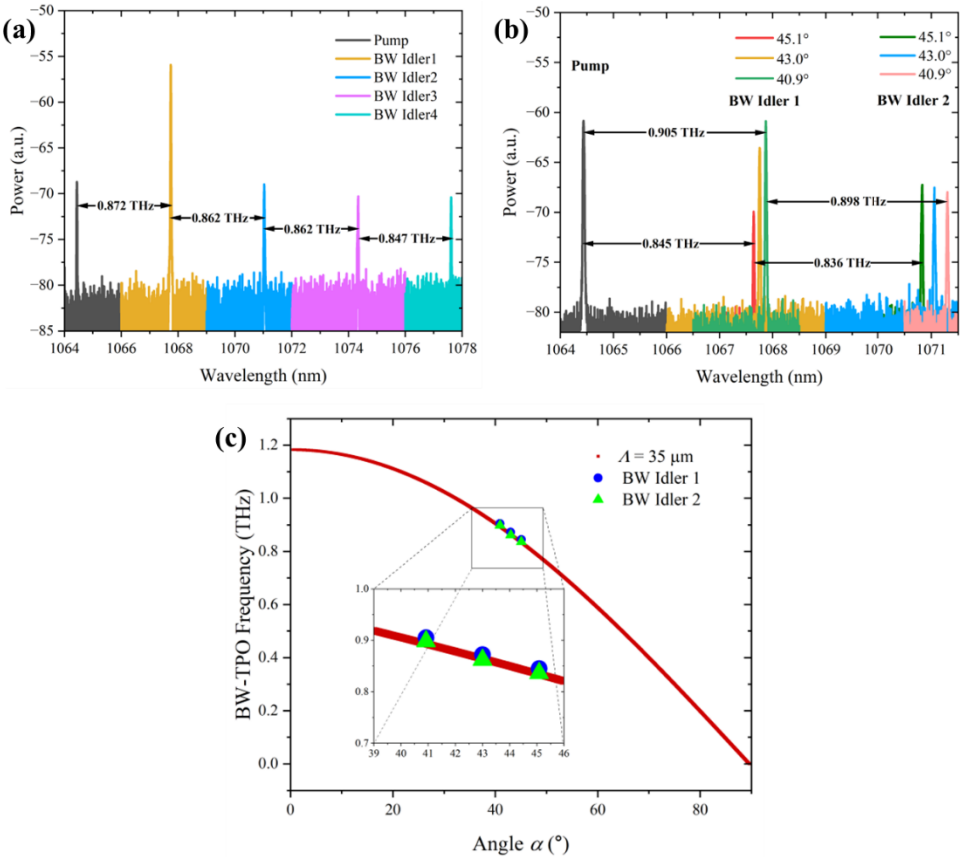

Fig. 2. (a) Spectra of the pump and backward idlers (BW Idler 1, 2, 3, and 4) with injection seeding. The presence of BW Idler 2 is due to the cascading process with BW Idler 1 as the new pump and a similar process ensues for the subsequent idler beams. (b) Angular tuning with α. Both first and second backward idlers exhibit tunability as α is changed from 40.9°- 45.1° resulting in an effective tunable range of 0.836–0.905 THz. (c) Experimental PPLN rotation results plotted against the calculated QCPM curve with angular tuning range zoomed in.

Further cascading ensued where another idler, BW Idler 3, formed at $\lambda = 1074.34$ nm with a corresponding spectral separation of $\Delta\omega_{BW3} = 0.862$ THz ($\lambda_{THz} = 348$ µm, rounded off). Injection seeding causes another idler, BW Idler 4, to appear at $\lambda = 1077.61$ nm with a spectral separation of $\Delta\omega_{BW4} = 0.847$ THz (($\lambda_{THz} = 354$ µm) from BW Idler 3, further proving the efficiency of the experimental system. Generally, the THz frequencies with each successive cascading process became lower, with differences as high as ~10 GHz. This is expected when compared to the calculated tuning curve in Fig. 1(d) and upon the extension of the phase-matching diagram to include the cascade process, Fig. 1(c); the momentum vectors of the idler and THz-waves change accordingly with each higher order cascading due to the adjustment in α and θ with the constant Λ. In addition, the idler beams also have narrow bandwidths like the pump, which is an inherent property of BW-TPO due to the absence of a cavity resonator [13,18]. The bandwidth for BW Idler1 is ~0.02 nm similar to the pump and with comparable bandwidths for the other idler beams. The emitted THz-waves have a high conversion efficiency due to the spectral overlap of Fourier

Optics EXPRESS

transform limited pulsed waves, enabling us to confirm the generation of the fourth-order idler wave.

3.2. Tunability

With a simple rotation of the PPLN crystal, the tunability of the oscillation frequency can also be observed and done for the unseeded case. From the original pump-to-grating vector angle of $\alpha = 43.0°$ at normal incidence, the PPLN was rotated by 4.5° in the clockwise and counter-clockwise directions, effectively changing α to range from 40.9° to 45.1° when accounting for refraction. With this rotation, related shifts in the idler spectra were observed (Fig. 2 (b)). At $\alpha = 40.9°$, BW Idler 1 swings to $\lambda = 1067.87$ nm, corresponding to $\Delta\omega_{BW1} = 0.905$ THz and $\lambda_{THz} = 331$ µm. At 45.1°, the spectral line shifted to $\lambda = 1067.64$ nm, equivalent to $\Delta\omega_{BW1} = 0.845$ THz ($\lambda_{THz} = 355$ µm) from the pump. The range in angle tunability gives a bandwidth of 60 GHz. Furthermore, similar shifts in BW Idler 2 are seen, with the spectral separation measured from BW Idler 1 at the same α. At $\alpha = 40.9°$, the spectra of BW Idler 2 shifted to $\lambda = 1071.30$ nm, corresponding to $\Delta\omega_{BW2} = 0.898$ THz ($\lambda_{THz} = 334$ µm). At 45.1°, the spectral line shifts to $\lambda = 1070.83$ nm, equivalent to $\Delta\omega_{BW2} = 0.836$ THz ($\lambda_{THz} = 359$ µm) and a tunable bandwidth of 62 GHz. Considering both idlers, the effective tunable range is 0.836–0.905 THz, which fits with the calculated BW-TPO tuning curve shown in Fig. 2(c). As per the calculations, this bandwidth can be broader with larger rotation angles. Similarly, as indicated earlier in the cascade process, when α is changed, a consequent angular shift in θ also follows, resulting in changes to the idler and THz-wave momentum vectors and in effect, to the corresponding wavelengths. The design parameters, such as the grating period and PPLN dimensions, limit the frequency tunability.

3.3. Pump energy dependence

The dependence of the THz-wave and idler beams on pump energy were measured at the original grating vector-to-pump angle $\alpha = 43.0°$, to determine the threshold peak intensities for BW-TPO and to assess the pump conversion efficiency of the process. For this set of measurements, the seed power was pegged at 100 mW while the pump energy varied from 4.50 mJ (start of seeded BW-Idler 1 detection) to 15.3 mJ with the results shown in Fig. 3. The individual idler energies for the main BW-TPO and cascaded processes, are plotted in Fig. 3(a) with the total idler energies for both seeded and unseeded case displayed separately (Fig. 3(b)) and the THz signal shown in Fig. 3(c). A linear increase in the idler energies is observed with increasing pump intensity beyond the threshold. From the linear part of the curve for BW Idler 1, the BW-TPO threshold was determined to be 9.67 mJ, equivalent to a peak intensity of 5.65 GW/cm^2 for the case without a seed beam. For the seeded case, the threshold energy (peak intensity) was at 5.25 mJ (3.06 GW/cm^2) for a reduction of 45.7% from the unseeded. In the case of BW Idler 2, its threshold was at 12.5 mJ (7.30 GW/cm^2) for the unseeded case, while for the seeded case was at 8.25 mJ (4.82 GW/cm^2) again reducing the threshold value. For BW Idler 3, the unseeded beam was initially detected at a pump energy of 15.0 mJ, while the seeded case was reduced to 10.8 mJ (6.28 GW/cm^2). The BW Idler 4, which appeared with seeding, had a threshold of 14.3 mJ (8.35 GW/cm^2). Also noted is that with the appearance of each cascaded idler, some of the energy transferred from the source idler, as indicated by the kink in each plot of the preceding BW idler, denoting that no back-conversion to the pump is present. A clearer trend of its linear increase is seen if the total idler vs. pump energy is considered (Fig. 3(b)). The conversion efficiency at the maximum pump energy of 15.25 mJ reached 12.3% without seeding and was as high as 18.3% with seeding, for an enhancement of 48.8%. The unseeded conversion efficiency is lower comparing previous results in [18], where a value of 15% was reported using a different PPLN crystal emitting at a BW-TPO frequency of 0.3 THz. From our measurements using THz time-domain spectroscopy, the absorption coefficients of LN were approximately 1.8 cm^{-1} and

Optics EXPRESS

8.8 cm^{-1} at 0.3THz and 0.87 THz, respectively. Based on this, it can be inferred qualitatively that the current PPLN design has a lower parametric gain due to a higher THz absorption loss.

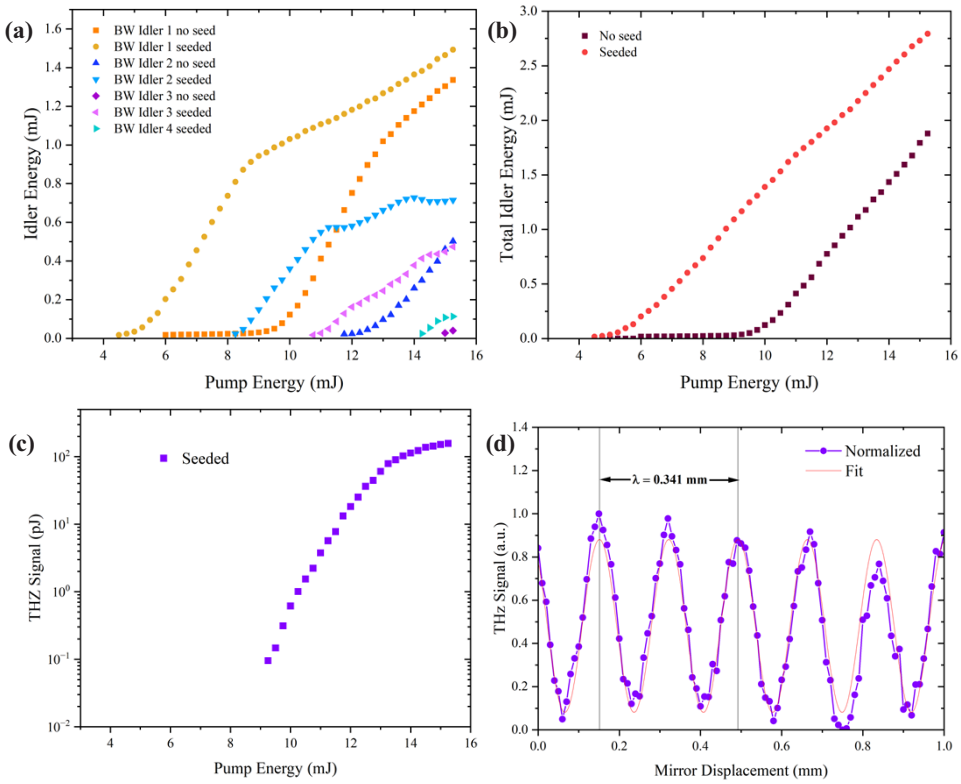

Fig. 3. (a) Pump energy dependence of the individual BW idler beam energies for the seeded and unseeded case. (b) Total BW idler beam energy as a function of pump energy showing monotonically increasing behavior for both unseeded and seeded cases. (c) THz signal vs. pump energy with the THz signal increasing with pump energy. (d) Interferogram of the seeded THz signal where an approximate wavelength of 0.341 mm equivalent to 0.878 THz was measured.

In contrast, the THz signal was first observed at a pump energy of 9.25 mJ in the seeded case and a direct proportionality is seen with increased pump energy (Fig. 3(c)). The peak energy at the maximum pump setting was 157 pJ. As for the unseeded case, the THz-wave can be detected only at the maximum pump energy, however, the signal was very weak (~0.15 pJ) so the variation with the pump energy is not presented. We attribute this disparity in the input-output characteristics between idler and THz waves to two factors: first, the limit of the THz detector sensitivity, where the corresponding signal levels (<0.15 pJ) at pump energies below 9.25 mJ are not detectable, and second, losses due to higher THz-wave absorption inside the PPLN at this frequency, where added power from injection-seeding was needed to boost the detection of the THz signal. Nevertheless, this generally agrees with the more than 1000x enhancement factor with the seeded case stated in [19]. The peak THz-wave output power corresponding to the maximum measured peak energy for this set of measurements was estimated to be around 365 mW, based on the FWHM pulse width of the idler/THz pulse that is typically half of that of the pump [18]. This value is orders of magnitude lower than the kW levels obtained from is-TPG [20], as well as from estimates for the 0.3 THz BW-TPO [18]. Though lower, this peak output power is still significant and expected bearing in mind the absorption loss at higher frequencies

Optics EXPRESS

and the shorter crystal length. To confirm the BW-TPO frequency, the interferogram was acquired (Fig. 3(d)) using a scanning Fabry-Perot etalon of a pair of partially reflecting silicon wafers. An approximate wavelength of 0.341 mm, equivalent to a frequency of 0.878 THz, was measured consistent with the BW-TPO QCPM calculations and the spectral separation indicated earlier, along with an estimated bandwidth of less than 11 GHz.

3.4. Seed power dependence

We also looked at the seed power dependence of the THz-wave and idler beams to investigate the effect of injection seeding with the pump energy set to 11.5 mJ (6.71 GW/cm^2) based on the linear trend of the THz signal in Fig. 3(c). However, aside from the first BW idler, note that BW Idlers 2 and 3 are also present at this pump energy making the system more complex than the cascadeless process. Total idler energy was considered instead as a function of seed power to account for this. Figure 4(a) shows how the individual idler energies behave with seed power. Overall, the idler energies increased during the first few seed power settings and then saturated at varying rates as the seed power increased. From the normalized total BW idler energy and THz signal outputs in Fig. 4(b), the THz signal monotonically increases with seed power. However, the total idler output saturates for seed powers above 250 mW. Considering the earlier findings on pump energy dependence where the unseeded THz-wave case was only detectable at maximum pump energy, we can conclude that within the PPLN crystal, the forward propagating idler wave is amplified via the optical parametric amplification effect until it reaches saturation. However, the backward propagating THz-waves, especially those generated by second- and higher order cascade processes, suffer absorption loss with less gain assistance as it exits, hence the need for seeding.

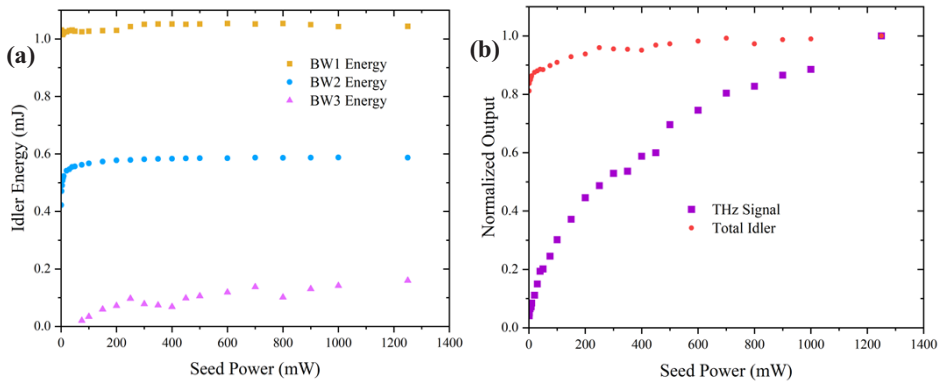

Fig. 4. (a) Seed power dependence of the individual BW idler beam energies at the pump energy of 11.5 mJ. (b) Normalized total idler and THz outputs as a function of seed power at the same pump energy setting.

4. Conclusion

The first demonstration of a frequency tunable BW-TPO centered at a high frequency of 0.87 THz is reported. Based on the QCPM scheme, a slant-stripe-type PPLN crystal was designed as the nonlinear medium for generating the backward oscillation at the target frequency. Upon excitation of this slant-stripe-type PPLN with a sub-nanosecond pulsed source of $\lambda = 1064.44$ nm, down-converted THz and idler beams were generated. The resulting first idler had a wavelength of 1067.75 nm, equivalent to an oscillation frequency of 0.872 THz, while interferogram measurements of the THz signal show consistent values. Additional idler beams were also

Optics EXPRESS

observed due to a cascading process. The BW-TPO frequency was angle-tuned by rotating the PPLN crystal and ranged from 0.836–0.905 THz. The threshold pump intensity for BW-TPO was determined to be 5.6 GW/cm^2 while obtaining a conversion efficiency as high as 12.3% at a pump energy (intensity) of 15.25 mJ (8.90 GW/cm^2). Injection seeding by a CW laser with the same first idler wavelength caused a reduction of the BW-TPO threshold energy by 45.7% and an improved pump-to-idler energy conversion efficiency value of 18.3%. As the seed power was increased, the THz output also increased while the total idler output exhibited saturation at higher seed powers. The tunable injection-seeded BW-TPO holds great potential as a simple and efficient THz light source for a wide range of applications.

Funding. Japan-China Scientific Cooperation Program between Japan Society for the Promotion of Science (JSPS) and National Natural Science Foundation of China (NSFC) (JPJSBP120207407); Innovative Science and Technology Initiative for Security, Acquisition, Technology & Logistics Agency, Japan (ATLA) (JPJ004596).

Acknowledgments. The authors would like to thank Prof. H. Ito of RIKEN/Tohoku University and Prof. M. Kumano of Tohoku University for fruitful discussions.

Disclosures. The authors declare that there are no conflicts of interest related to this article.

Data availability. Data underlying the results presented in this paper are not publicly available at this time but may be obtained from the authors upon reasonable request.

References

1. M. Tonouchi, "Cutting-edge terahertz technology," Nat. Photonics **1**(2), 97–105 (2007).
2. D. Mittleman, "Perspective: Terahertz science and technology," J. Appl. Phys. **122**(23), 230901 (2017).
3. K. M. S. Huq, S. A. Busari, J. Rodriguez, V. Frascolla, W. Bazzi, and D. C. Sicker, "Terahertz-Enabled Wireless System for Beyond-5 G Ultra-Fast Networks: A Brief Survey," IEEE Network **33**(4), 89–95 (2019).
4. H. -J. Song and N. Lee, "Terahertz Communications: Challenges in the Next Decade," IEEE Trans. Terahertz Sci. Technol. **12**(2), 105–117 (2022).
5. A. Boes, L. Chang, C. Langrok, M. Yu, M. Zhang, Q. Lin, M. Lončar, M. Fejer, J. Bowers, and A. Mitchell, "Lithium niobate photonics: Unlocking the electromagnetic spectrum," Science **379**(6627), eabj4396 (2023).
6. B. Zhang, Z. Ma, J. Ma, X. Wu, C. Ouyang, D. Kong, T. Hong, X. Wang, P. Yang, L. Chen, Y. Li, and J. Zhang, "1.4-mJ High Energy Terahertz Radiation from Lithium Niobates," Laser Photonics Rev. **15**(3), 2000295 (2021).
7. J. Kiessling, R. Sowade, I. Breunig, K. Buse, and V. Dierolf, "Cascaded optical parametric oscillations generating tunable terahertz waves in periodically poled lithium niobate crystals," Opt. Express **17**(1), 87–91 (2009).
8. T. D. Wang, S. T. Lin, Y. Y. Lin, A. C. Chiang, and Y. C. Huang, "Forward and backward Terahertz-wave difference-frequency generations from periodically poled lithium niobate," Opt. Express **16**(9), 6471–6478 (2008).
9. K. Murate and K. Kawase, "Perspective: Terahertz wave parametric generator and its applications," J. Appl. Phys. **124**(16), 160901 (2018).
10. S. E. Harris, "Proposed backward wave oscillation in the infrared," Appl. Phys. Lett. **9**(3), 114–116 (1966).
11. Y. J. Ding and J. B. Khurgin, "Backward optical parametric oscillators and amplifiers," IEEE J. Quantum Electron. **32**(9), 1574–1582 (1996).
12. Y. J. Ding and J. B. Khurgin, "A new scheme for efficient generation of coherent and incoherent submillimeter to THz waves in periodically-poled lithium niobate," Opt. Commun. **148**(1-3), 105–109 (1998).
13. Canalias and V. Pasiskevicius, "Mirrorless optical parametric oscillator," Nat. Photonics **1**(8), 459–462 (2007).
14. G. Strömqvist, V. Pasiskevicius, C. Canalias, P. Aschieri, A. Picozzi, and C. Montes, "Temporal coherence in mirrorless optical parametric oscillators," J. Opt. Soc. Am. B **29**(6), 1194 (2012).
15. A. Liljestrand, V. Zukauskas, C. Pasiskevicius, and Canalias, "Highly efficient mirrorless optical parametric oscillator pumped by nanosecond pulses," Opt. Lett. **42**(13), 2435–2438 (2017).
16. R. S. Coetzee, A. Zukauskas, C. Canalias, and V. Pasiskevicius, "Low-threshold, mid-infrared backward-wave parametric oscillator with periodically poled Rb:KTP," APL Photonics **3**(7), 071302 (2018).
17. A. L. Viotti, A. Zukauskas, C. Canalias, F. Laurell, and V. Pasiskevicius, "Narrowband, tunable, infrared radiation by parametric amplification of a chirped backward-wave OPO signal," Opt. Express **27**(8), 10602–10610 (2019).
18. K. Nawata, Y. Tokizane, Y. Takida, and H. Minamide, "Tunable Backward Terahertz-wave Parametric Oscillation," Sci. Rep. **9**(1), 726 (2019).
19. Y. Takida, K. Nawata, and H. Minamide, "Injection-seeded backward terahertz-wave parametric oscillator," APL Photonics **5**(6), 061301 (2020).
20. H. Minamide, S. Hayashi, K. Nawata, T. Taira, J. Shikata, and K. Kawase, "Kilowatt-peak Terahertz-wave Generation and Sub-femtojoule Terahertz-wave Pulse Detection Based on Nonlinear Optical Wavelength-conversion at Room Temperature," J. Infrared, Millimeter, Terahertz Waves **35**(1), 25–37 (2014).